

Electronic correlation strength of inorganic electriles from first principles

Shu Kanno¹, Tomofumi Tada^{1,*}, Takeru Utsumi¹, Kazuma Nakamura², Hideo Hosono^{1,†}

¹ *Materials Research Center for Element Strategy, Tokyo Institute of Technology, 4259 Nagatsuta, Midori-ku, Yokohama 226-8503, Japan*

² *Quantum Physics Section, Department of Basic Sciences, Kyushu Institute of Technology, 1-1 Sensui-cho, Tobata, Kitakyushu, Fukuoka 804-8550, Japan*

* tada.t.ae@m.titech.ac.jp

† hosono@mces.titech.ac.jp

Abstract

We present a systematic study clarifying an electronic correlation trend of electriles from first principles. By using the maximally localized Wannier function and the constrained random phase approximation, we calculated the electronic correlation strength $(U - U_{nn})/|t|$ of 19 inorganic electriles, where U , U_{nn} , and t are the effective onsite Coulomb repulsion, nearest-neighbor Coulomb repulsion, and the nearest-neighbor transfer integrals, respectively. The electronic correlation was found to be highly correlated with the dimensionality of the Wannier-function network of anionic electrons in electriles; the correlation strength varies in the order $0D \gg 1D > 2D \sim 3D$, showing good correspondence with experimental trends, and exceeds 10 (a measure for the emergence of exotic properties) in all the 0D systems and some of the 1D materials. We also found that the electronic correlation depends on the cation species surrounding the anionic electrons; in the 1D electriles, the electronic correlation becomes stronger for cationic walls consisting of Ca^{2+} , Sr^{2+} , and Ba^{2+} in this order, and the correlation strength exceeds 10 for Ba_5As_3 . The theoretical results indicate that 0- and 1-dimensional electriles will be new research targets for studies on strongly correlated electron systems.

I. INTRODUCTION

Strongly correlated electron systems, represented by Mott insulators, have attracted attention as a platform for the emergence of exotic properties such as high-Tc

superconductivity [1,2]. In general, strongly correlated electron systems are focused on *d*- and *f*-electron systems, and “electronic correlation strength” has been introduced to represent the strength of the electronic correlation [3]. For example, the electronic correlation strength can be a measure of the possibility of the metal-insulator transition in transition metal compounds; the strength of NiO is larger than that of TiO by a factor of four, and the former becomes an insulator with large energy band splitting and the latter a metal [4]. Recently, correlated electron behavior has been observed in a novel materials group, *electrides*, in which *s*-electrons confined in sub-nanometer-sized spaces with different shapes (voids, channels, and interlayer spaces) in intrinsic crystal structures behave like anions (the confined electron is called an anionic electron) [5–13].

The first confirmed electride is the organic crystal $\text{Cs}^+(18\text{-crown-6})_2\text{:e}^-$ synthesized by Ellaboudy *et al.* in 1983 [5]. However, the organic electride is so chemically and thermally unstable that research on its properties remains unveiled. An inorganic electride that is superior to organic electrides in terms of stability was synthesized by Matsuishi *et al.* in 2003 as $[\text{Ca}_{24}\text{Al}_{28}\text{O}_{64}]^{4+}(4\text{e}^-)$ (hereafter referred to as C12A7:e⁻) [6]. C12A7:e⁻ has *s*-electrons confined in crystallographic cages composed of Ca^{2+} , Al^{3+} , and O^{2-} . C12A7:e⁻ shows a metal-insulator transition when the electron concentration exceeds $\sim 2 \times 10^{21} \text{ cm}^{-3}$ [14], and the metallic samples exhibit BCS-type superconductivity [15]. In addition to C12A7:e⁻, various types of inorganic electrides have been discovered. For example, Ca_2N is a two-dimensional electride in which anionic electrons are sandwiched by cationic slabs $[\text{Ca}_2\text{N}]^+$ and behave as a two-dimensional (2D) electron gas [7]. Another interesting example is Sr_5P_3 , a one-dimensional (1D) electride showing Mott insulating behavior; the anionic electrons are confined in channels with Sr^{2+} walls [11]. Thus, electrides are a group of materials that exhibit a variety of properties ranging from insulators to metals. Although the electronic correlation in electrides has been discussed individually [11,12,16–18], a systematic analysis of the electronic correlation of electrides has not been conducted. It is of interest to know the electronic correlation strength for *s*-electrons confined in crystallographic sub-nanometer-sized spaces to gain a comprehensive understanding of the electronic interaction in condensed matter.

In this study, we calculate the electronic correlation strength of inorganic electrides by using first-principles electronic structure calculations. The target systems are 19 inorganic electrides and are classified in terms of the Wannier function framework of anionic electrons, creating an easy-to-understand classification as zero-dimensional (0D), 1D, 2D, and three-dimensional (3D) electrides. Based on this classification, we will show the correspondence between the electronic correlation strength and the electron confinement spaces.

II. METHODS

The electronic correlation strength is calculated as $(U - U_{nn})/|t|$, where U is the effective on-site Coulomb repulsion, U_{nn} is the effective nearest-neighbor Coulomb repulsion, and $|t|$ is the absolute value of the nearest-neighbor transfer integral. The electronic correlation strength can be used to investigate the trend in the electronic correlation of materials. When the kinetic energy is significantly larger than the potential energy, i.e., $(U - U_{nn})/|t| \ll 1$, the electrons are itinerant throughout the system (i.e., metal). In contrast, when $(U - U_{nn})/|t| \gg 1$, electrons tend to be localized and dominated by the potential energy (i.e., the system becomes a Mott insulator involving magnetic ordering). In the intermediate region, the kinetic energy and potential energy of electrons compete with each other, leading to interesting phenomena. For example, the electronic correlation strengths of 3*d*-cuprates, the parent materials of high-*T*_c superconductors, are known to be ~ 7 [19,20].

In the present study, we calculate the electronic correlation strength of various electriles and investigate the theoretical trend for the electronic correlation of electriles. For this purpose, we calculate the physical parameters $|t|$, U , and U_{nn} from first principles based on the procedure given in Fig. 1(a). We demonstrate a concrete procedure for Na-electro-sodalite Na₈(AlSiO₄)₆, having well bounded anionic electrons in nanospaces.

In Step I, we perform a density-functional band-structure calculation. The resulting eigenvalues and eigenstates of the Kohn-Sham Hamiltonian are used for the subsequent maximally localized Wannier function calculations (Step II). To obtain the Wannier function for the anionic electron orbital, we set an energy window including the target bands for the Wannier functions, which is set to 3.5 - 4.8 eV in this example. We use an *s*-type Gaussian function centered at the nanospace as the initial guess for the Wannier function calculations. With these settings, the Wannier functions are obtained by minimizing the spread functional [21] and/or the spillage functional for the band-entangled situation [22]. The transfer parameter is determined from matrix elements of the Kohn-Sham Hamiltonian in the Wannier functions as

$$t_{ij} = \int_V \Psi_i(\mathbf{r})^* H_0 \Psi_j(\mathbf{r}) d\mathbf{r}, \quad (1)$$

where H_0 is the Kohn-Sham Hamiltonian, $\Psi_i(\mathbf{r})$ is the i th Wannier function, and the integral is taken for the crystal volume V . The nearest-neighbor transfer integral t is determined as the matrix element between the nearest-neighbor pair of Wannier functions.

The upper panel in Fig. 1(b) compares the original density-functional band structure (red solid curves) with the Wannier interpolated band (blue crosses) of Na-electro-sodalite, from which we confirm good agreement between the two bands. The lower panel in Fig. 1(b) shows the calculated real-space Wannier function, from which the well-localized character of the sodalite Wannier function in the nanospace is confirmed. The calculated nearest transfer energy $|t|$ is 55 meV.

In Step III, we calculate the effective on-site U and nearest-neighbor U_{nn} Coulomb repulsions with the Wannier functions. The effective direct Coulomb integral is defined as

$$U_{ij} = \iint_V W(\mathbf{r}, \mathbf{r}') |\Psi_i(\mathbf{r})|^2 |\Psi_j(\mathbf{r}')|^2 d\mathbf{r} d\mathbf{r}', \quad (2)$$

where $W(\mathbf{r}, \mathbf{r}')$ is the screened Coulomb interaction based on the constrained random phase approximation (cRPA) [1,23–26]. U is evaluated as the average of the diagonal components of U_{ij} . In the sodalite, the values of U and U_{nn} are 2.86 eV and 0.66 eV, respectively, and thus $(U - U_{nn})/|t|$ is obtained as 39.8. Since the value of the strength is quite large, the sodalite is classified as a strongly correlated material [27]. We performed the calculations for U , U_{nn} , $|t|$, and $(U - U_{nn})/|t|$ of 19 electrides.

As a preprocessing before Step I, full optimization of the crystal structures of the electrides was carried out using VASP [28,29], and for the relaxed structures we performed xTAPP band calculations [30,31] to generate inputs for RESPACK [24,32–36] that calculates the maximally localized Wannier function and the cRPA screened Coulomb interaction. We used the Perdew-Burke-Ernzerhof type [37] for the exchange-correlation functional in both the VASP and xTAPP calculations. For core electrons, the projector augmented wave (PAW) method in VASP and the norm-conserving pseudopotential in xTAPP were adopted. The wave function cut-off, dielectric function cut-off, k -point grid, and the number of bands used for each material were determined so that the differences in U converged within 0.1 eV (The values of each parameter are listed in Table A1 of supplemental material A).

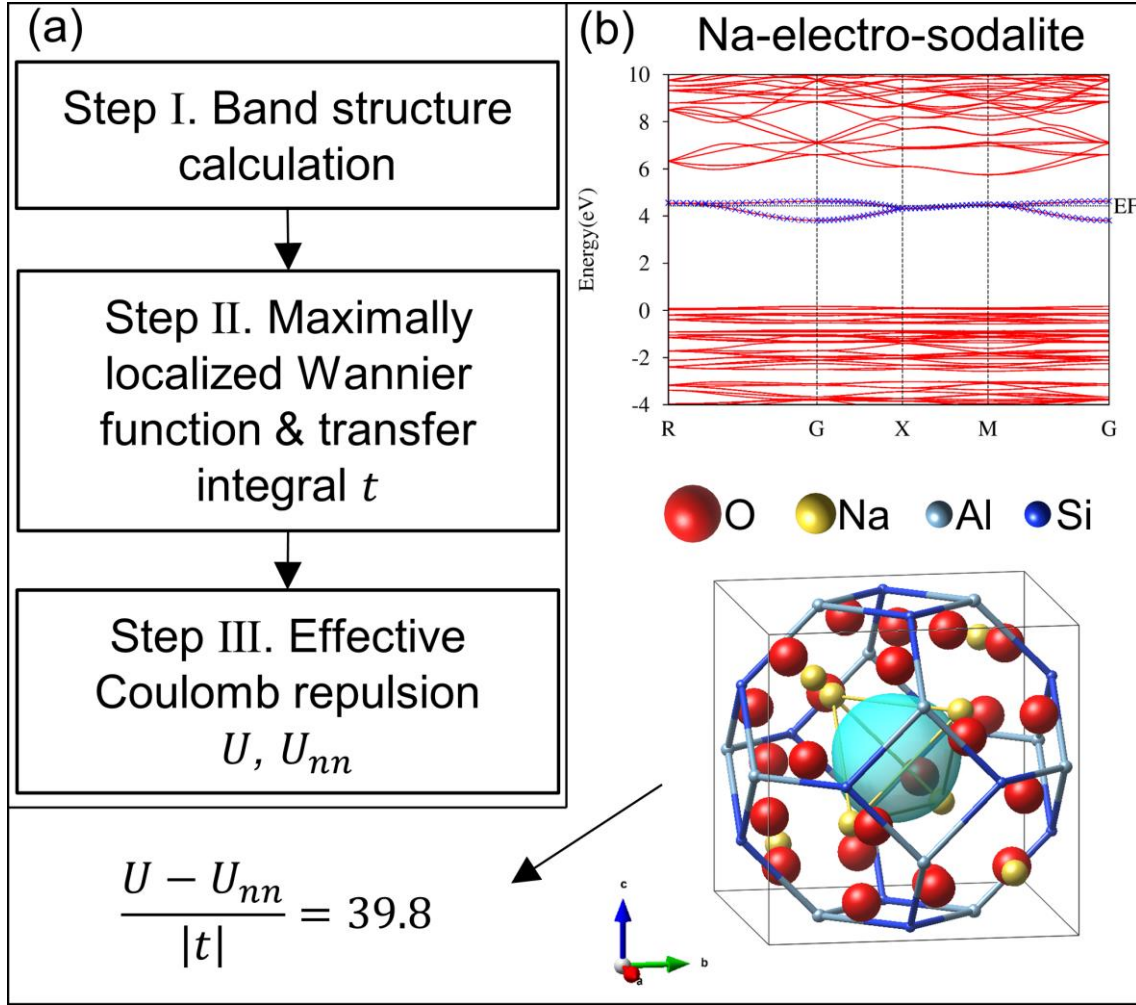
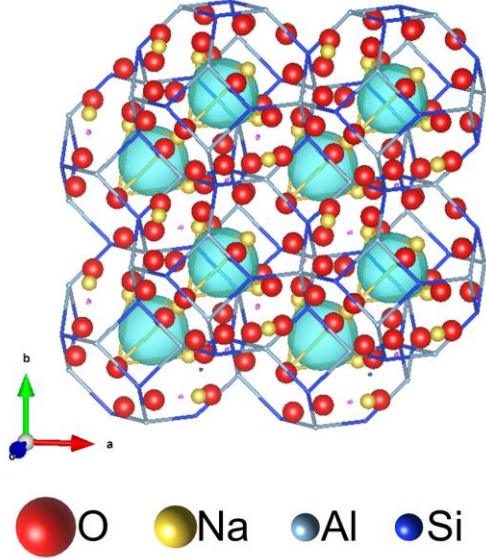


FIG. 1. Computational flow of electronic structure calculations to derive effective parameters and the electronic correlation strength of anionic electrons. (a) Flow chart showing the three steps: (Step I) density-functional band calculation, (Step II) calculations for maximally localized Wannier function and transfer integral t [Eq. (1)], and (Step III) calculations for effective on-site U and nearest-neighbor U_{nn} Coulomb repulsions, based on cRPA [Eq. (2)]. (b) Upper panel: A comparison between the calculated density-functional band structure (red solid curves) and the Wannier interpolated bands (blue crosses) for the anionic electrons of Na-electro-sodalite. EF represents the Fermi energy. Lower panel: Calculated real-space Wannier function (isosurface of 0.04) for the anionic electron (light blue) drawn by VESTA [38]. With the resulting values of $|t| = 55$ meV, $U = 2.86$ eV, and $U_{nn} = 0.66$ eV, the correlation strength of the sodalite is calculated as 39.8.

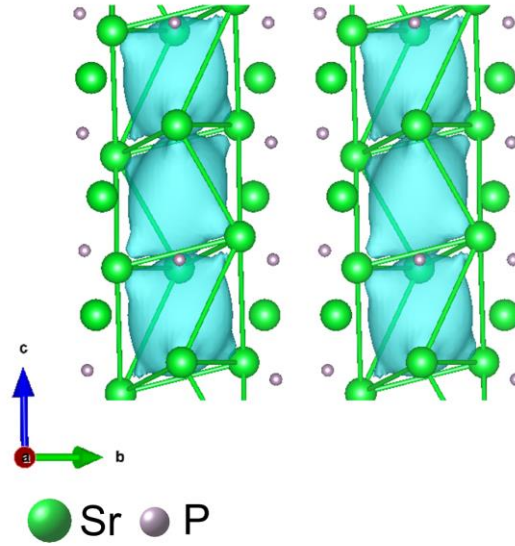
III. RESULTS

Before showing the calculation results for the electronic correlation strength of electrides, we describe a classification of the present electrides in terms of the dimensionality of the Wannier-function network of anionic electrons. Figure 2 shows examples of the electrides classified by the dimension of the Wannier-function-network: (a) Na-electro-sodalite (0D), (b) Sr_5P_3 (1D), (c) Ca_2N (2D), and (d) LaH_2 (3D). In the 0D electrides, each Wannier function is confined in a cage and has no connection to adjacent Wannier functions. In the 1D case, the Wannier functions have connections along a particular direction. Similarly, in the 2D case, the Wannier functions form layers, and each layer is separated by a nanolayer block. In the 3D case, the Wannier functions create a 3D network. For electrides, hybridization between the Wannier orbital of the anionic electrons and the atomic orbitals of the cages plays an important role in network formation. In the case of LaH_2 [Fig. 2(d)], the anionic electron orbital is hybridized with the La-*d* orbital, resulting in a 3D network of Wannier functions. The dimensionality of the Wannier-function network is quite useful for understanding the low-energy properties of the electride, as explained later.

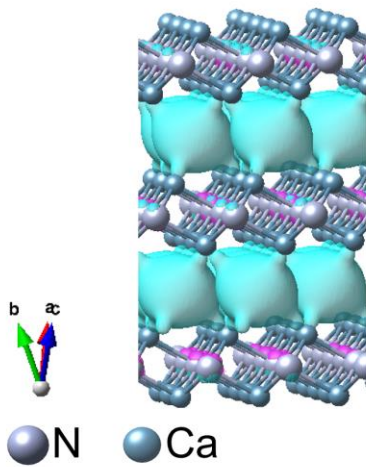
(a) Na-electro-sodalite, 0D



(b) Sr_5P_3 , 1D



(c) Ca_2N , 2D



(d) LaH_2 , 3D

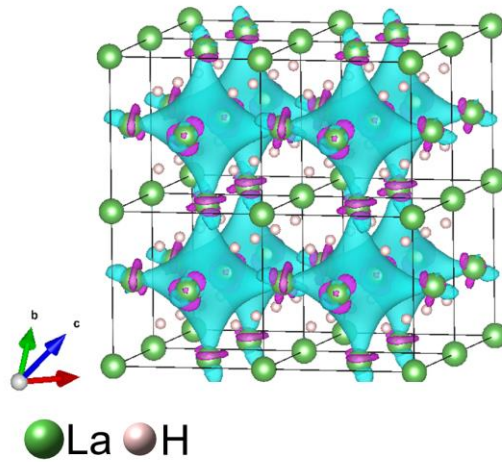


FIG. 2 Classification of Wannier-function network from dimensionality: (a) Na-electro-sodalite (0D), (b) Sr_5P_3 (1D), (c) Ca_2N (2D), and (d) LaH_2 (3D). In these panels, we display the Wannier functions for multiple unit cells to show the connectivity of the Wannier functions. Note that the Wannier function itself has a localized nature in the unit cell. The isosurfaces are 0.04.

Figure 3 shows the calculated correlation strength $(U - U_{nn})/|t|$ of 19 electriles, together with the U , U_{nn} , and $|t|$ parameters. The calculated values are given in Table A2 in supplemental material A. We confirm an appreciable material dependence for the correlation strength; the differences in the Wannier-function networks bring about big differences in the correlation strength. From the figure, we find that the correlation strength varies in the order $0D \gg 1D > 2D \sim 3D$; the strengths of the 0D systems are larger than 10, while those of the 2D and 3D systems are smaller than 3. Thus, it is expected that the 0D electriles would exhibit strong correlation effects such as the realization of Mott insulators and magnetic states, while the 2D and 3D electriles would be metals or band insulators because the anionic electrons behave like free electrons. The observed trend of the correlation strength on the dimensionality is consistent with experiments [6,7,10,11,39].

There are also some remarkable trends. In the 1D electriles, the correlation strength of the Ca_5Pn_3 ($\text{Pn}=\text{P}, \text{As}, \text{Sb}$) group is smaller than that of the Sr_5Pn_3 group, and that of the latter group is smaller than that of the Ba_5Pn_3 group. For example, the values of 1D Ca_5P_3 , Sr_5P_3 , and Ba_5P_3 are 4.0, 5.7, and 9.7, respectively, and thus 1D Ba_5Pn_3 ($\text{Pn}=\text{P}, \text{As}, \text{Sb}$) will be of interest for future experimental studies since 1D Sr_5P_3 has already been shown to be a Mott insulator. The increasing trend in correlation strength, $\text{Ca}_5\text{Pn}_3 < \text{Sr}_5\text{Pn}_3 < \text{Ba}_5\text{Pn}_3$, originates from the decreasing trend in the transfer integrals $|t|$ according to $\text{Ca}_5\text{Pn}_3 > \text{Sr}_5\text{Pn}_3 > \text{Ba}_5\text{Pn}_3$ (see Fig. 3). The 1D Ae_5Pn_3 ($\text{Ae}=\text{Ca}, \text{Sr}, \text{Ba}$) electriles have a hexagonal structure, and the Wannier functions form a 1D network along the c axis. Therefore, the transfer integrals $|t|$ depend sensitively on the c parameter of the system. The c parameters of Ca_5P_3 , Sr_5P_3 , and Ba_5P_3 are 6.89 Å, 7.46 Å, and 8.07 Å, respectively, and the transfer integrals are 164, 129, and 58 meV, respectively. Thus, the cation species in 1D Ae_5Pn_3 has a considerable effect on the strength of the electronic correlation via the transfer $|t|$.

Besides, in the 0D electriles, we identified a group having considerably small Coulomb interactions and transfer integrals: Ae_5Sb_3 with the Yb_5Sb_3 structure ($U = 0.76$ eV, $U_{nn} = 0.14$ eV, and $|t| = 21$ meV on average). To understand the trend in 0D Ae_5Sb_3 , Fig. 4 compares the band structure for 0D Sr_5Sb_3 [panel (a)] with that for 0D C12A7:e^- [panel (b)] having considerably large values of $U = 2.63$ eV, $U_{nn} = 0.89$ eV, and $|t| = 113$ meV. It can be seen that Sr_5Sb_3 has a fairly dense band structure in contrast to the sparse band structure of C12A7:e^- . Because of the dense band structure, screening due to low-energy excitation becomes effective in Sr_5Sb_3 , so that the resulting effective Coulomb interactions are significantly reduced. In addition, the Wannier bandwidths

calculated for Sr_5Sb_3 and C12A7:e^- are 0.6 eV and 1.7 eV, respectively, leading to a small $|t|$ for Sr_5Sb_3 . We emphasize that the 0D Ae_5Sb_3 group is still a strongly correlated electron system having large correlation strengths of more than 10 despite the small values of U , U_{nn} , and $|t|$.

Finally, we remark on the weak correlation trend in the 2D and 3D electrides. As can be seen from Figs. 2(c) and 2(d), the electrides have large spaces where electrons can move freely, and thus the electrides can have a large kinetic energy. Thus, the electronic correlation would not be strong in the 2D and 3D electrides. For 2D electrides, good 2D electron gas confinement can occur between the two-dimensional layers. Recently, a material with a large thermoelectric coefficient has been found in a 2D electron gas system [40], and research on such a system would be interesting for the study of electrides (the thermoelectric properties of 0D C12A7:e^- have been already reported [41]). 3D electrides are actually quite similar to 0D electrides; the difference is that the 0D anionic electrons are well isolated [Fig.2(a)], whereas, in the 3D system, the anionic electrons are spatially spread through hybridization with neighboring orbitals of anionic electrons. [Fig. 2(d)]. Therefore, by changing the cation walls, it might be possible to control the electronic correlation in 0D and 3D electrides in the weak-correlation to strong-correlation regimes, which is important for verifying strong correlation phenomena such as metal-insulator transitions [42].

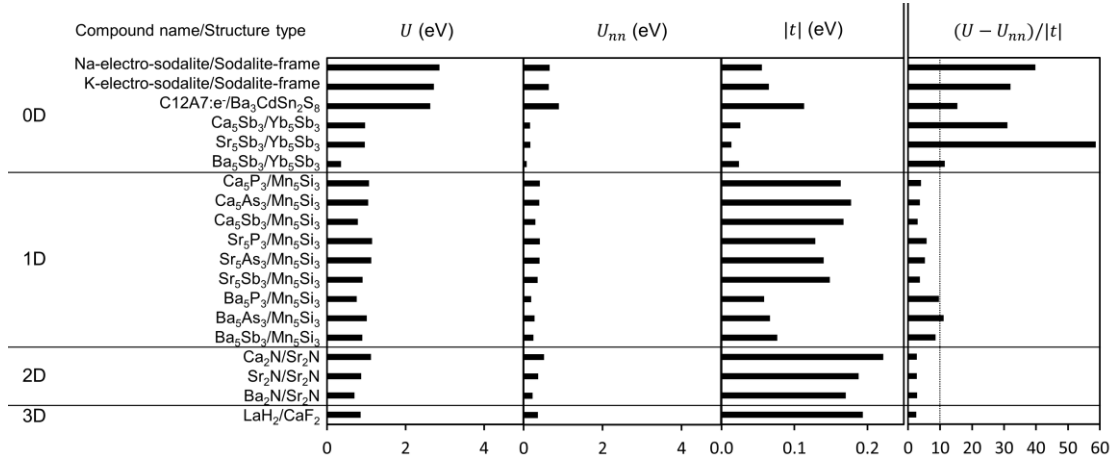


FIG. 3. Comparative chart of calculated cRPA onsite U and nearest-neighbor U_{nn} Coulomb interactions [Eq. (2)], nearest-neighbor transfer integral $|t|$ [Eq. (1)], and electronic correlation strength $(U - U_{nn})/|t|$ of 19 inorganic electrides including 0D, 1D, 2D, and 3D systems. The dotted line for $(U - U_{nn})/|t| = 10$ is given as a guide, which is a rough threshold for the appearance of strong correlation phenomena. The crystal structures of all the structure types used in this study are shown in Fig. A1 and Table A3 of supplemental material A.

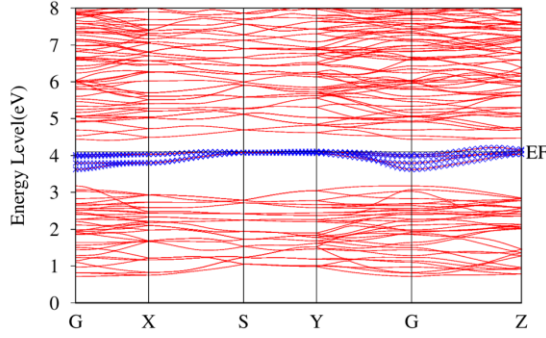
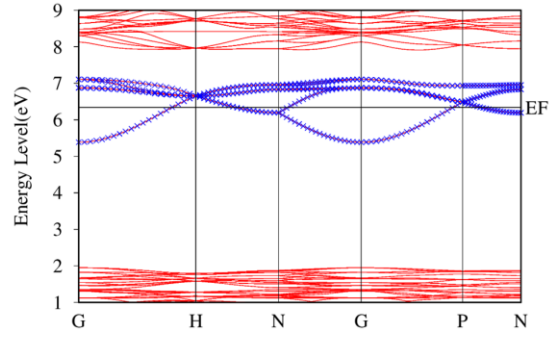
(a) 0D Sr_5Sb_3 (b) C12A7:e⁻

FIG. 4. Calculated density-functional band structures (red solid curves) and Wannier interpolated bands (blue crosses) for anionic electrons in (a) 0D Sr_5Sb_3 and (b) 0D C12A7:e⁻. EF is the Fermi level. Band dispersions are plotted along the high symmetry points, where $G = (0, 0, 0)$, $X = (a^*/2, 0, 0)$, $S = (a^*/2, b^*/2, 0)$, $Y = (0, b^*/2, 0)$, $Z = (0, 0, c^*/2)$, $H = (-a^*/2, b^*/2, c^*/2)$, $N = (0, 0, c^*/2)$, and $P = (a^*/4, b^*/4, c^*/4)$, with a^* , b^* , and c^* being the basis vectors of the reciprocal lattice.

IV. CONCLUSION

In summary, we present a first-principles analysis of electronic correlation of inorganic electrides. In the present study, we classified the electrides from the viewpoint of the electronic structure, focusing on the Wannier-function network of anionic electrons. The network analysis is effective for obtaining a systematic understanding of the electronic correlation of electrides. We derived the transfer integral $|t|$ and effective interaction parameters U and U_{nn} using the maximally localized Wannier function and cRPA for 19 electrides, including 0D, 1D, 2D, and 3D systems. Through comparison of the electronic correlation strength $(U - U_{nn})/|t|$ of the electrides, we found that the 0D electrides and some of the 1D electrides exhibit strong electronic correlation, while the higher dimensional electrides basically exhibit weaker electronic correlation dominated by the gain of kinetic energy in free space. The trend of the electronic correlation on the dimensionality is consistent with experimental observations.

The present analysis proposes practical ideas for controlling the electronic properties of electrides. By controlling and designing the nanospaces in electrides, bandwidth control is possible. This is particularly important for 1D electrides, where the bandwidth depends sensitively on the type of cations. Thus, they would be expected to be prototype electrides for investigating correlation phenomena such as metal-insulator and magnetic transitions. Also, accurate filling control for the electrides is important for further study; 0D $C_{12}A_7:e^-$ has 0.7 electrons per crystalline void and 2D Y_2C [9,43] has 1.8 electrons per void. They are not half-filling, and the observation of strong correlation phenomena by doping control would be expected.

ACKNOWLEDGMENTS

This work was supported by funds from Kakenhi Grant-in-Aid (No. 17H06153) from the Japan Society for the Promotion of Science (JSPS) and the Ministry of Education, Culture, Sports, Science and Technology (MEXT) Element Strategy Initiative to form a research core (No. JPMXP0112101001). K.N. acknowledges the financial support of JSPS Kakenhi Grant No. 16H06345, No. 16K05452, No. 17H03393, No. 17H03379, and No. 19K03673.

References

- [1] M. Imada and T. Miyake, *Electronic Structure Calculation by First Principles for Strongly Correlated Electron Systems*, J. Phys. Soc. Jpn. **79**, 112001 (2010).
- [2] G. Kotliar and D. Vollhardt, *Strongly Correlated Materials: Insights From Dynamical Mean-Field Theory*, Phys. Today **57**, 53 (2004).
- [3] M. Imada, A. Fujimori, and Y. Tokura, *Metal-Insulator Transitions*, Rev. Mod. Phys. **70**, 1039 (1998).
- [4] A. E. Bocquet, T. Mizokawa, K. Morikawa, A. Fujimori, S. R. Barman, K. Maiti, D. D. Sarma, Y. Tokura, and M. Onoda, *Electronic Structure of Early 3d-Transition-Metal Oxides by Analysis of the 2p Core-Level Photoemission Spectra*, Phys. Rev. B **53**, 1161 (1996).
- [5] A. Ellaboudy, J. L. Dye, and P. B. Smith, *Cesium 18-Crown-6 Compounds. A Crystalline Cesium and a Crystalline Electride*, J. Am. Chem. Soc. **105**, 6490 (1983).
- [6] S. Matsuishi, Y. Toda, M. Miyakawa, K. Hayashi, T. Kamiya, M. Hirano, I. Tanaka, and H. Hosono, *High-Density Electron Anions in a Nanoporous Single Crystal: $[Ca_{24}Al_{28}O_{64}]^{4+}(4e^-)$* , Science **301**, 626 (2003).
- [7] K. Lee, S. W. Kim, Y. Toda, S. Matsuishi, and H. Hosono, *Dicalcium Nitride as a Two-Dimensional Electride with an Anionic Electron Layer*, Nature **494**, 336 (2013).
- [8] T. Tada, S. Takemoto, S. Matsuishi, and H. Hosono, *High-Throughput Ab Initio Screening for Two-Dimensional Electride Materials*, Inorg. Chem. **53**, 10347 (2014).
- [9] T. Inoshita, S. Jeong, N. Hamada, and H. Hosono, *Exploration for Two-Dimensional Electrifies via Database Screening and Ab Initio Calculation*, Phys. Rev. X **4**, 031023 (2014).
- [10] H. Mizoguchi, M. Okunaka, M. Kitano, S. Matsuishi, T. Yokoyama, and H. Hosono, *Hydride-Based Electride Material, LnH_2 ($Ln = La, Ce, \text{ or } Y$)*, Inorg. Chem. **55**, 8833 (2016).
- [11] J. Wang, K. Hanzawa, H. Hiramatsu, J. Kim, N. Umezawa, K. Iwanaka, T. Tada, and H. Hosono, *Exploration of Stable Strontium Phosphide-Based Electrifies: Theoretical Structure Prediction and Experimental Validation*, J. Am. Chem. Soc. **139**, 15668 (2017).
- [12] Y. Lu, J. Wang, J. Li, J. Wu, S. Kanno, T. Tada, and H. Hosono, *Realization of Mott-Insulating Electrifies in Dimorphic Yb_5Sb_3* , Phys. Rev. B **98**, 125128 (2018).

- [13] H. Hosono and M. Kitano, *Advances in Materials and Applications of Inorganic Electrides*, Chem. Rev. **121**, 3121 (2021).
- [14] S. W. Kim, S. Matsuishi, T. Nomura, Y. Kubota, M. Takata, K. Hayashi, T. Kamiya, M. Hirano, and H. Hosono, *Metallic State in a Lime-Alumina Compound with Nanoporous Structure*, Nano Lett. **7**, 1138 (2007).
- [15] M. Miyakawa, S. W. Kim, M. Hirano, Y. Kohama, H. Kawaji, T. Atake, H. Ikegami, K. Kono, and H. Hosono, *Superconductivity in an Inorganic Electride $12\text{CaO}\cdot 7\text{Al}_2\text{O}_3:e^-$* , J. Am. Chem. Soc. **129**, 7270 (2007).
- [16] D. Y. Novoselov, V. I. Anisimov, and A. R. Oganov, *Strong Electronic Correlations in Interstitial Magnetic Centers of Zero-Dimensional Electride $\beta\text{-Yb}_5\text{Sb}_3$* , Phys. Rev. B **103**, 235126 (2021).
- [17] J. Zhou, Y. P. Feng, and L. Shen, *Atomic-Orbital-Free Intrinsic Ferromagnetism in Electrenes*, Phys. Rev. B **102**, 180407 (2020).
- [18] Y. Nohara, K. Nakamura, and R. Arita, *Ab Initio Derivation of Correlated Superatom Model for Potassium Loaded Zeolite A*, J. Phys. Soc. Jpn. **80**, 124705 (2011).
- [19] M. Hirayama, T. Miyake, M. Imada, and S. Biermann, *Low-Energy Effective Hamiltonians for Correlated Electron Systems beyond Density Functional Theory*, Phys. Rev. B **96**, 075102 (2017).
- [20] T. Ohgoe, M. Hirayama, T. Misawa, K. Ido, Y. Yamaji, and M. Imada, *Ab Initio Study of Superconductivity and Inhomogeneity in a Hg-Based Cuprate Superconductor*, Phys. Rev. B **101**, 045124 (2020).
- [21] N. Marzari and D. Vanderbilt, *Maximally Localized Generalized Wannier Functions for Composite Energy Bands*, Phys. Rev. B **56**, 12847 (1997).
- [22] I. Souza, N. Marzari, and D. Vanderbilt, *Maximally Localized Wannier Functions for Entangled Energy Bands*, Phys. Rev. B **65**, 035109 (2001).
- [23] F. Aryasetiawan, M. Imada, A. Georges, G. Kotliar, S. Biermann, and A. I. Lichtenstein, *Frequency-Dependent Local Interactions and Low-Energy Effective Models from Electronic Structure Calculations*, Phys. Rev. B **70**, 195104 (2004).
- [24] K. Nakamura, Y. Yoshimoto, Y. Nomura, T. Tadano, M. Kawamura, T. Kosugi, K. Yoshimi, T. Misawa, and Y. Motoyama, *RESPACK: An Ab Initio Tool for Derivation of Effective Low-Energy Model of Material*, Comput. Phys. Commun. **261**, 107781 (2021).
- [25] K. Ido, Y. Motoyama, K. Yoshimi, and T. Misawa, *Data Analysis on Ab Initio*

Effective Hamiltonians of Iron-Based Superconductors, arXiv:2109.09121.

- [26] T. Miyake, K. Nakamura, R. Arita, and M. Imada, *Comparison of Ab Initio Low-Energy Models for LaFePO, LaFeAsO, BaFe₂As₂, LiFeAs, FeSe, and FeTe: Electron Correlation and Covalency*, J. Phys. Soc. Jpn. **79**, 044705 (2010).
- [27] K. Nakamura, T. Koretsune, and R. Arita, *Ab Initio Derivation of the Low-Energy Model for Alkali-Cluster-Loaded Sodalites*, Phys. Rev. B **80**, 174420 (2009).
- [28] G. Kresse and J. Hafner, *Ab Initio Molecular Dynamics for Liquid Metals*, Phys. Rev. B **47**, 558 (1993).
- [29] G. Kresse and J. Hafner, *Ab Initio Molecular-Dynamics Simulation of the Liquid-Metal-Amorphous-Semiconductor Transition in Germanium*, Phys. Rev. B **49**, 14251 (1994).
- [30] O. Sugino and A. Oshiyama, *Vacancy in Si: Successful Description within the Local-Density Approximation*, Phys. Rev. Lett. **68**, 1858 (1992).
- [31] J. Yamauchi, M. Tsukada, S. Watanabe, and O. Sugino, *First-Principles Study on Energetics of c-BN(001) Reconstructed Surfaces*, Phys. Rev. B **54**, 5586 (1996).
- [32] K. Nakamura, Y. Nohara, Y. Yosimoto, and Y. Nomura, *Ab Initio GW plus Cumulant Calculation for Isolated Band Systems: Application to Organic Conductor TMTSF)₂PF₆ and Transition-Metal Oxide SrVO₃*, Phys. Rev. B **93**, 085124 (2016).
- [33] K. Nakamura, Y. Yoshimoto, T. Kosugi, R. Arita, and M. Imada, *Ab Initio Derivation of Low-Energy Model for κ -ET Type Organic Conductors*, J. Phys. Soc. Jpn. **78**, 083710 (2009).
- [34] K. Nakamura, R. Arita, and M. Imada, *Ab Initio Derivation of Low-Energy Model for Iron-Based Superconductors LaFeAsO and LaFePO*, J. Phys. Soc. Jpn. **77**, 093711 (2008).
- [35] Y. Nohara, S. Yamamoto, and T. Fujiwara, *Electronic Structure of Perovskite-Type Transition Metal Oxides LaMO₃ (Ti~Cu) by U+GW Approximation*, Phys. Rev. B **79**, 195110 (2009).
- [36] T. Fujiwara, S. Yamamoto, and Y. Ishii, *Generalization of the Iterative Perturbation Theory and Metal–Insulator Transition in Multi-Orbital Hubbard Bands*, J. Phys. Soc. Jpn. **72**, 777 (2003).
- [37] J. P. Perdew, K. Burke, and M. Ernzerhof, *Generalized Gradient Approximation Made Simple*, Phys. Rev. Lett. **77**, 3865 (1996).
- [38] K. Momma and F. Izumi, *VESTA 3 for Three-Dimensional Visualization of Crystal*,

Volumetric and Morphology Data, J. Appl. Crystallogr. **44**, 1272 (2011).

- [39] V. I. Srdanov, G. D. Stucky, E. Lippmaa, and G. Engelhardt, *Evidence for an Antiferromagnetic Transition in a Zeolite-Supported Cubic Lattice of F Centers*, Phys. Rev. Lett. **80**, 2449 (1998).
- [40] H. Ohta, S. Kim, Y. Mune, T. Mizoguchi, K. Nomura, S. Ohta, T. Nomura, Y. Nakanishi, Y. Ikuhara, M. Hirano, H. Hosono, and K. Koumoto, *Giant Thermoelectric Seebeck Coefficient of a Two-Dimensional Electron Gas in SrTiO₃*, Nat. Mater. **6**, 129 (2007).
- [41] S. W. Kim, R. Tarumi, H. Iwasaki, H. Ohta, M. Hirano, and H. Hosono, *Thermal Conductivity and Seebeck Coefficient of 12CaO · 7Al₂O₃ Electride with a Cage Structure*, Phys. Rev. B **80**, 075201 (2009).
- [42] R. Arita, T. Miyake, T. Kotani, M. van Schilfhaarde, T. Oka, K. Kuroki, Y. Nozue, and H. Aoki, *Electronic Properties of Alkali-Metal Loaded Zeolites: Supercrystal Mott Insulators*, Phys. Rev. B **69**, 195106 (2004).
- [43] X. Zhang, Z. Xiao, H. Lei, Y. Toda, S. Matsuishi, T. Kamiya, S. Ueda, and H. Hosono, *Two-Dimensional Transition-Metal Electride Y₂C*, Chem. Mater. **26**, 6638 (2014).

Supplementary Material

Electronic correlation strength of inorganic electriles

from first principles

Shu Kanno¹, Tomofumi Tada^{1,*}, Takeru Utsumi¹, Kazuma Nakamura²,
Hideo Hosono^{1,†}

¹*Materials Research Center for Element Strategy, Tokyo Institute of Technology, 4259
Nagatsuta, Midori-ku, Yokohama 226-8503, Japan*

²*Quantum Physics Section, Department of Basic Sciences, Kyushu Institute of
Technology, 1-1 Sensui-cho, Tobata, Kitakyushu, Fukuoka, 804-8550, Japan*

* tada.t.ae@m.titech.ac.jp

† hosono@mces.titech.ac.jp

A. Computational conditions and calculated results

Table A1 lists the detailed computational conditions, and Table A2 the calculated results for U , U_{nn} , $|t|$, and $(U - U_{nn})/|t|$, where U is the effective on-site Coulomb repulsion, U_{nn} is the effective nearest-neighbor Coulomb repulsion, and $|t|$ is the absolute value of the nearest-neighbor transfer integral. We obtained the crystal structural data by using the Materials Project [1] database and Inorganic Crystal Structure Database (ICSD) [2], as listed in the column “Reference” in Tables A1 and A2. When the column is blank, the structures of the systems were prepared based on an experimentally confirmed compound in the same structure type. Figure A1 shows the crystal structures for all the structure types used in this study, and Table A3 shows the lattice and structure parameters of the crystal structures.

TABLE A1

The computational conditions for all the compounds calculated in this study

Dimension	Compound	Structure type	Wave function cut-off (eV)	k -point grid	Number of bands	Dielectric function cutoff (eV)	Reference
0D	Na-electro-sodalite	Sodalite-frame	81	7x7x7	300	3	[1]
0D	K-electro-sodalite	Sodalite-frame	49	5x5x5	200	5	[2]
0D	C12A7:e ⁻	Ba ₃ CdSn ₂ S ₈	81	6x6x6	350	3	[1]
0D	Ca ₅ Sb ₃	Yb ₅ Sb ₃	81	5x5x5	240	3	[2]
0D	Sr ₅ Sb ₃	Yb ₅ Sb ₃	81	5x5x5	240	3	[2]
0D	Ba ₅ Sb ₃	Yb ₅ Sb ₃	81	5x5x5	240	3	
1D	Ca ₅ P ₃	Mn ₅ Si ₃	81	5x5x5	120	3	
1D	Ca ₅ As ₃	Mn ₅ Si ₃	81	5x5x5	120	3	[2]
1D	Ca ₅ Sb ₃	Mn ₅ Si ₃	81	5x5x5	160	3	[2]
1D	Sr ₅ P ₃	Mn ₅ Si ₃	50	7x7x9	120	5	[3]
1D	Sr ₅ As ₃	Mn ₅ Si ₃	81	5x5x5	160	3	[2]
1D	Sr ₅ Sb ₃	Yb ₅ Sb ₃	81	5x5x5	240	3	
1D	Ba ₅ P ₃	Mn ₅ Si ₃	81	5x5x5	160	3	
1D	Ba ₅ As ₃	Mn ₅ Si ₃	81	5x5x5	160	3	[2]
1D	Ba ₅ Sb ₃	Yb ₅ Sb ₃	81	5x5x5	240	3	[2]
2D	Ca ₂ N	Sr ₂ N	81	8x8x8	60	1.5	[1]
2D	Sr ₂ N	Sr ₂ N	81	8x8x8	60	3	[1]
2D	Ba ₂ N	Sr ₂ N	81	8x8x8	60	3	[1]
3D	LaH ₂	CaF ₂	81	11x11x11	50	3	[1]

TABLE A2

Calculated U , U_{nn} , $|t|$, and $(U - U_{nn})/|t|$ of all the compounds calculated in this study

Dimension	Compound	Structure type	U (eV)	U_{nn} (eV)	$ t $ (eV)	$\frac{U - U_{nn}}{ t }$	Reference
0D	Na-electro-sodalite	Sodalite-frame	2.86	0.66	0.055	39.8	[1]
0D	K-electro-sodalite	Sodalite-frame	2.72	0.64	0.065	32.0	[2]
0D	C12A7:e ⁻	Ba ₃ CdSn ₂ S ₈	2.63	0.89	0.113	15.4	[1]
0D	Ca ₅ Sb ₃	Yb ₅ Sb ₃	0.97	0.17	0.026	31.1	[2]
0D	Sr ₅ Sb ₃	Yb ₅ Sb ₃	0.96	0.17	0.014	58.7	[2]
0D	Ba ₅ Sb ₃	Yb ₅ Sb ₃	0.35	0.08	0.024	11.5	
1D	Ca ₅ P ₃	Mn ₅ Si ₃	1.07	0.41	0.164	4.0	
1D	Ca ₅ As ₃	Mn ₅ Si ₃	1.05	0.40	0.178	3.7	[2]
1D	Ca ₅ Sb ₃	Mn ₅ Si ₃	0.79	0.30	0.167	2.9	[2]
1D	Sr ₅ P ₃	Mn ₅ Si ₃	1.15	0.41	0.129	5.7	[3]
1D	Sr ₅ As ₃	Mn ₅ Si ₃	1.13	0.40	0.140	5.2	[2]
1D	Sr ₅ Sb ₃	Mn ₅ Si ₃	0.90	0.35	0.149	3.7	
1D	Ba ₅ P ₃	Mn ₅ Si ₃	0.76	0.19	0.058	9.7	
1D	Ba ₅ As ₃	Mn ₅ Si ₃	1.01	0.27	0.067	11.1	[2]
1D	Ba ₅ Sb ₃	Mn ₅ Si ₃	0.90	0.25	0.076	8.5	[2]
2D	Ca ₂ N	Sr ₂ N	1.12	0.51	0.222	2.7	[1]
2D	Sr ₂ N	Sr ₂ N	0.87	0.37	0.188	2.7	[1]
2D	Ba ₂ N	Sr ₂ N	0.70	0.22	0.170	2.8	[1]
3D	LaH ₂	CaF ₂	0.85	0.36	0.194	2.5	[1]

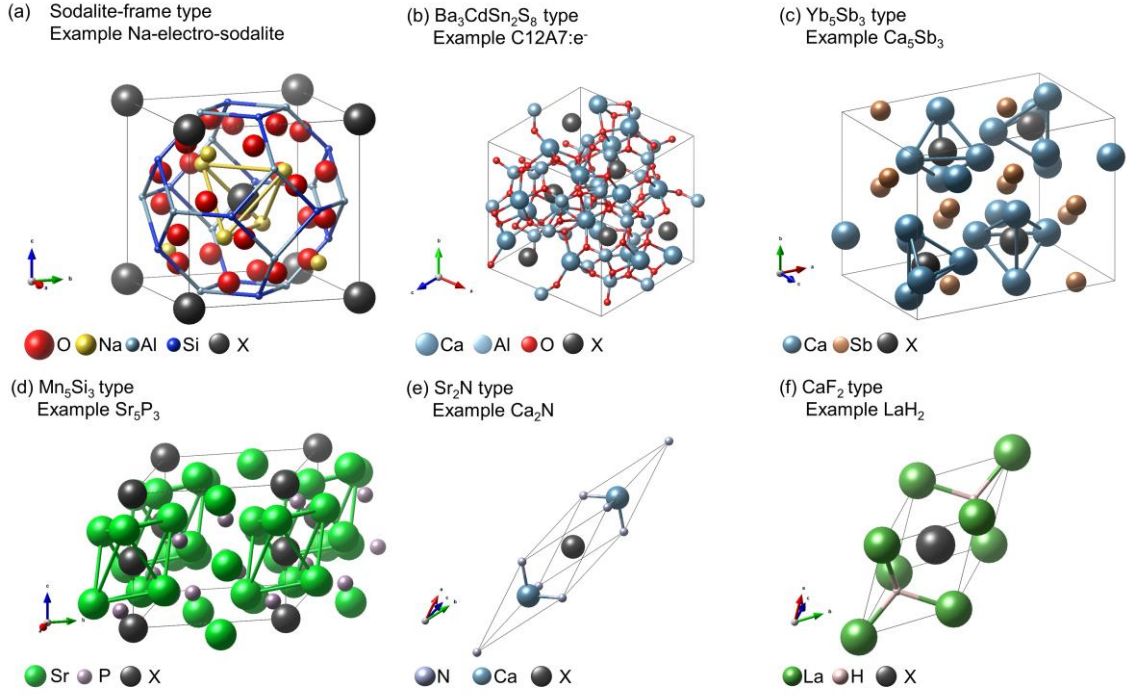


FIG. A1. Crystal structures of all the structure types used in this study. “X” represents the central position of the Wannier function; the positions can be changed slightly during the Wannier function optimization.

TABLE A3. Lattice and structure parameters of the crystal structures of all the structure types used in this study. We show the parameters for the examples of the compounds corresponding to each structure type. The fractional coordinate of “X” represents the central position of the Wannier function for the initial guess in the optimization.

Structure type	Dimension	Example	Lattice parameter	Structure parameter			
				Atom	Fractional coordinate		
					x	y	z
Sodalite-frame	0D	Na-electro-sodalite	$a=8.943\text{\AA}$	Al	0.250	0.000	0.500
			$b=8.943\text{\AA}$	Al	0.750	0.000	0.500
			$c=8.943\text{\AA}$	Al	0.500	0.250	0.000
			$\alpha=90^\circ$	Al	0.500	0.750	0.000
			$\beta=90^\circ$	Al	0.000	0.500	0.250
			$\gamma=90^\circ$	Al	0.000	0.500	0.750
				Si	0.250	0.500	0.000
	Si	0.750	0.500	0.000			

				Si	0.000	0.250	0.500
				Si	0.000	0.750	0.500
				Si	0.500	0.000	0.250
				Si	0.500	0.000	0.750
				Na	0.176	0.176	0.176
				Na	0.824	0.824	0.176
				Na	0.824	0.176	0.824
				Na	0.176	0.824	0.824
				Na	0.676	0.676	0.676
				Na	0.324	0.324	0.676
				Na	0.676	0.324	0.324
				Na	0.324	0.676	0.324
				O	0.152	0.435	0.140
				O	0.849	0.565	0.140
				O	0.849	0.435	0.860
				O	0.152	0.565	0.860
				O	0.140	0.152	0.435
				O	0.140	0.849	0.565
				O	0.860	0.849	0.435
				O	0.860	0.152	0.565
				O	0.435	0.140	0.152
				O	0.565	0.140	0.849
				O	0.435	0.860	0.849
				O	0.565	0.860	0.152
				O	0.935	0.652	0.640
				O	0.065	0.349	0.640
				O	0.935	0.349	0.360
				O	0.065	0.652	0.360
				O	0.652	0.640	0.935
				O	0.349	0.640	0.065
				O	0.349	0.360	0.935
				O	0.652	0.360	0.065
				O	0.640	0.935	0.652
				O	0.640	0.065	0.349
				O	0.360	0.935	0.349

				O	0.360	0.065	0.652
				X	0.000	0.000	0.000
				X	0.500	0.500	0.500
Ba ₃ CdSn ₂ S ₈	0D	C12A7:e ⁻	a=10.479Å	Ca	0.640	0.250	0.890
			b=10.479Å	Ca	0.860	0.750	0.610
			c=10.479Å	Ca	0.390	0.750	0.140
			α=109.471°	Ca	0.110	0.250	0.360
			β=109.471°	Ca	0.890	0.640	0.250
			γ=109.471°	Ca	0.610	0.860	0.750
				Ca	0.140	0.390	0.750
				Ca	0.360	0.110	0.250
				Ca	0.250	0.890	0.640
				Ca	0.750	0.610	0.860
				Ca	0.750	0.140	0.390
				Ca	0.250	0.360	0.110
				Al	0.375	0.250	0.625
				Al	0.125	0.750	0.875
				Al	0.625	0.375	0.250
				Al	0.875	0.125	0.750
				Al	0.250	0.625	0.375
				Al	0.750	0.875	0.125
				Al	0.500	0.000	0.037
				Al	0.037	0.500	0.000
				Al	0.000	0.037	0.500
				Al	0.464	0.464	0.464
				Al	0.537	0.500	0.000
				Al	0.500	0.000	0.537
				Al	0.000	0.537	0.500
				Al	0.964	0.964	0.964
				O	0.500	0.000	0.871
	O	0.871	0.500	0.000			
	O	0.000	0.871	0.500			
	O	0.629	0.629	0.629			
	O	0.371	0.500	0.000			
	O	0.500	0.000	0.371			

				O	0.000	0.371	0.500
				O	0.129	0.129	0.129
				O	0.408	0.094	0.617
				O	0.523	0.406	0.814
				O	0.092	0.709	0.686
				O	0.977	0.791	0.883
				O	0.117	0.594	0.908
				O	0.314	0.906	0.023
				O	0.186	0.209	0.592
				O	0.383	0.291	0.477
				O	0.617	0.408	0.094
				O	0.814	0.523	0.406
				O	0.686	0.092	0.709
				O	0.883	0.977	0.791
				O	0.908	0.117	0.594
				O	0.023	0.314	0.906
				O	0.592	0.186	0.209
				O	0.477	0.383	0.291
				O	0.094	0.617	0.408
				O	0.406	0.814	0.523
				O	0.709	0.686	0.092
				O	0.791	0.883	0.977
				O	0.594	0.908	0.117
				O	0.906	0.023	0.314
				O	0.209	0.592	0.186
				O	0.291	0.477	0.383
				X	0.625	0.750	0.375
				X	0.750	0.375	0.625
				X	0.375	0.625	0.750
				X	0.875	0.250	0.125
				X	0.125	0.875	0.250
				X	0.250	0.125	0.875
Yb ₅ Sb ₃	0D	Ca ₅ Sb ₃	a=12.502Å	Ca	0.075	0.043	0.693
			b=9.512Å	Ca	0.925	0.958	0.307
			c=8.287Å	Ca	0.425	0.958	0.193

			$\alpha=90^\circ$	Ca	0.575	0.043	0.807
			$\beta=90^\circ$	Ca	0.925	0.543	0.307
			$\gamma=90^\circ$	Ca	0.075	0.458	0.693
				Ca	0.575	0.458	0.807
				Ca	0.425	0.543	0.193
				Ca	0.228	0.250	0.321
				Ca	0.773	0.750	0.679
				Ca	0.273	0.750	0.821
				Ca	0.728	0.250	0.179
				Ca	0.289	0.250	0.852
				Ca	0.711	0.750	0.149
				Ca	0.211	0.750	0.352
				Ca	0.789	0.250	0.649
				Ca	0.506	0.250	0.465
				Ca	0.494	0.750	0.536
				Ca	0.994	0.750	0.965
				Ca	0.006	0.250	0.036
				Sb	0.170	0.985	0.067
				Sb	0.830	0.015	0.933
				Sb	0.330	0.015	0.567
				Sb	0.670	0.985	0.433
				Sb	0.830	0.485	0.933
				Sb	0.170	0.515	0.067
				Sb	0.670	0.515	0.433
				Sb	0.330	0.485	0.567
				Sb	0.983	0.250	0.422
				Sb	0.017	0.750	0.578
				Sb	0.517	0.750	0.922
				Sb	0.483	0.250	0.078
				X	0.112	0.250	0.818
				X	0.612	0.250	0.682
				X	0.388	0.750	0.318
				X	0.888	0.750	0.182
Mn ₅ Si ₃	1D	Sr ₅ P ₃	a=8.696Å	Sr	0.741	0.998	0.199
			b=8.696Å	Sr	0.002	0.259	0.801

			c=7.464Å	Sr	0.259	0.002	0.801
			$\alpha=90.679^\circ$	Sr	0.998	0.741	0.199
			$\beta=90.679^\circ$	Sr	0.351	0.649	0.000
			$\gamma=119.480^\circ$	Sr	0.649	0.351	0.000
				Sr	0.685	0.315	0.500
				Sr	0.315	0.685	0.500
				Sr	0.255	0.255	0.331
				Sr	0.745	0.745	0.669
				P	0.609	0.999	0.767
				P	0.001	0.391	0.233
				P	0.391	0.001	0.233
				P	0.999	0.609	0.767
				P	0.393	0.393	0.728
				P	0.607	0.607	0.272
				X	0.000	0.000	0.000
				X	0.000	0.000	0.500
Sr ₂ N	2D	Ca ₂ N	a=6.747Å	Ca	0.268	0.268	0.268
			b=6.747Å	Ca	0.732	0.732	0.732
			c=6.747Å	N	0.000	0.000	0.000
			$\alpha=31.029^\circ$	X	0.500	0.500	0.500
			$\beta=31.029^\circ$				
			$\gamma=31.029^\circ$				
CaF ₂	3D	LaH ₂	a=3.999Å	La	0.000	0.000	0.000
			b=3.999Å	H	0.750	0.750	0.750
			c=3.999Å	H	0.250	0.250	0.250
			$\alpha=60^\circ$	X	0.500	0.500	0.500
			$\beta=60^\circ$				
			$\gamma=60^\circ$				

References

- [1] A. Jain, S. P. Ong, G. Hautier, W. Chen, W. D. Richards, S. Dacek, S. Cholia, D. Gunter, D. Skinner, G. Ceder, and K. A. Persson, *Commentary: The Materials Project: A Materials Genome Approach to Accelerating Materials Innovation*, *APL Materials* **1**, 011002 (2013).

- [2] G. Bergerhoff, I. D. Brown, F. Allen, and Others, *Crystallographic Databases*, International Union of Crystallography, Chester **360**, 77 (1987).
- [3] J. Wang, K. Hanzawa, H. Hiramatsu, J. Kim, N. Umezawa, K. Iwanaka, T. Tada, and H. Hosono, *Exploration of Stable Strontium Phosphide-Based Electrides: Theoretical Structure Prediction and Experimental Validation*, *J. Am. Chem. Soc.* **139**, 15668 (2017).